Journal of Nuclear Materials 376 (2008) 201–206

Contents lists available at ScienceDirect

Journal of Nuclear Materials

journal homepage: www.elsevier.com/locate/jnucmat

Characterization of monazite glass–ceramics as wasteform for simulated α-HLLW

Yong He *, Yanjie Lü, Qian Zhang

Materials Science and Chemical Engineering College, China University of Geosciences, Wuhan 430074, PR China

ARTICLE INFO

Article history:
Received 29 January 2007
Accepted 9 January 2008

PACS:
28.41.Kw

ABSTRACT

Two monazite glass–ceramic wasteforms were sintered by mixing the lanthanum metaphosphate glass powder with the oxide powder of the components in simulated α-HLWs. The co-existence of components Al and Mo in an iron phosphate melt separated the melt into two immiscible glass melts, namely aluminum iron phosphate glass (Gb) and molybdenum iron phosphate glass (Gg). 24 wt% of ZrO_2, together with P_2O_5 and proper amounts of Fe and Mo formed a zirconium pyrophosphate glass (Gg1), which was immiscible with the phase Gg. The iron ions in the wasteforms were all in Fe^{3+}, 1/3 of which was in 4-fold coordination. The O/P and O/(P + 1/3Fe^{3+}) ratios for the glass phases were Gg1 3.70, Gb 3.89–3.98, Gg 4.23–4.25, and Gg1 3.58, Gb 3.47–3.42, Gg 3.74–3.69, respectively. The dissolution rates of two wasteforms were 0.3008 and 0.2598 g/m^2d, respectively.

1. Introduction

High-level liquid wastes (HLLW), even though partitioned, are generally a multi-component complex system, therefore it is impossible for different HLLWs to be immobilized by the same approach. In Table 1 is shown the composition of a partitioned α-HLLW in Sichuan province, China, which was in a state of nitrate solution. The α-HLLW was changed by microwave technique into an alpha high-level waste (α-HLW) in the form of oxide powder.

Glass–ceramics, a host for HLLW, are composed of both crystalline phase(s) and a glass matrix with high chemical durability. Monazite, which not only contains U and Th, but hosts transuranium elements (TRUs), has extra high chemical and radioactive durabilities [1,2]. Regrettably, monazite was so selective [1,3] as not to host any other component like Mo, Zr, Fe in the HLW as shown in Table 1 except for the elements in lanthanum and actinide series. However, phosphate glasses could easily solidify all the components in HLWs without any selection. Hence what matters here is to select a highly durable glass matrix for a monazite glass–ceramic wasteform.

It was indicated in the previous studies of the iron phosphate glass as a HLW wasteform that the pyrophosphate glass (O/P = 3.5) had the highest chemical durability [4–8]. But, any glass always tends to crystallize spontaneously. Once its crystallization occurred, a pyrophosphate glass would be dissolved into both the orthophosphate crystals and a metaphosphate glass, the latter of which would greatly deteriorate the chemical durability of the wasteform. Therefore, raising the transition temperature (T_g) of the glass wasteform could retard or deter the spontaneous crystallization of the glasses. It was also shown in the study [9] that T_g in the phosphate glass would rise higher with its O/P ratio (mole) of phosphate glasses. Hitherto, no phosphate glass, which enjoys an O/P ratio of 4 without any crystallization, has been fabricated through traditional glass-making approaches.

The α-decays from TRUs would cause radioactive damage to crystalline and glass phases in the wasteform at the same time. Monazite phase has strong resistance to radioactive damage [1], but the resistance of ZrP_2O_7 phase to radioactive damage is unknown at present. The radioactive damage to glasses caused by the α-decay is shown in the volume expansion of the glasses and the formation of He bubbles and microcracks in the glasses [10–12], both of which altered the properties of the glasses and deteriorated the durability of the wasteform. There are much less data about radioactive damage from iron phosphate glass wasteforms than that from borosilicate glass ones.

In this study, the oxide powder of the components in simulated HLWs and the lanthanum metaphosphate glass powder were properly mixed to fabricate the two monazite glass–ceramic wasteforms, in which one of the phosphate glasses had an O/P ratio of more than 4, and Al and Mo resulted in the formation of immiscible phosphate glasses.

2. Experimental procedures

Most part of lanthanum and actinide elements were immobilized in monazite phase, but, as pointed out by the distribution law, small part of them would exist in the co-existence of glass phase and other crystalline phases, if any. Simulating method was adopted to study the distributions of the radioactive

* Corresponding author. Tel.: +86 027 62604302.
E-mail address: heyongyu@263.net (Y. He).

0022-3115/$ - see front matter © 2008 Elsevier B.V. All rights reserved.
doi:10.1016/j.jnucmat.2008.01.027

Table 1
Composition of α-HLLW (wt%)

Fe	La	Ce	Nd	Mo	Zr	TRU[a]	Total
5.59	9.64	12.76	33.52	8.22	0.16	30.10	100.00

[a] Transuranium elements.

components of the α-HLLW in wasteforms. The three criteria, namely same valence, similar ion radius and similar electron configurations, were observed for selecting surrogates for transuranium elements. According to the criteria there were detailed discussions in Refs. [13,14] of the analogy of Hf and Nd with TRUs and possibility of the substitutions of Hf^{4+} and Nd^{3+} for TRU^{4+} and TRU^{3+} in glass wasteforms. Considering Zr as an isomorphical substitute for Hf [15] and Zr, one of fission products, as one of important components in some kind of HLLW [16], Nd^{3+} and Zr^{4+} were used in this paper to simulate TRU^{3+} and TRU^{4+}, respectively so as to understand possible distributions of TRU^{3+} and TRU^{4+} in the phases of the wasteforms for subsequent hot experiments.

In this study, Zr^{4+} and Nd^{3+} were substituted for TRUs by way of equal mole to form 1# HLW and 2# HLW, respectively; and component Nd in the HLWs was substituted for La and Ce according to La/Ce mole ratio. In Table 2, the compositions of two simulated HLWs are listed.

The lanthanum metaphosphate glass powder, a raw material for wasteforms, consisted of La_2O_3 32 and P_2O_5 68 wt%. La_2O_3 powder and H_3PO_4 liquid, well-prepared in weight, were mixed to the consistency of paste and then dried at 450 °C so as to form a glass precursor. The glass precursor in an alumina crucible was melted at 1230 °C for 45 min before it was poured into cold water to gain colorless transparent lanthanum metaphosphate glass, and at the same time component Al in the crucible was introduced into the lanthanum metaphosphate glass when the glass was melted. The chemicals used in this experiment were all reagent-grade.

The wasteforms for 1# and 2# HLWs were named 1# wasteform (W1) and 2# wasteform (W2), respectively. Component P_2O_5 in wasteforms was introduced by the lanthanum metaphosphate glass. The ratios of the oxide powder of simulated α-HLW and the powder of lanthanum metaphosphate glass in 1W and 2W were 51:49 and 52:48 (wt%), respectively. The batch of each wasteform, to which were added 1 wt% of methyl cellulose as bond and the proper amount of deionized water, was mixed evenly, then pressed into several discs with a diameter of 45 mm and a thickness of 5 mm at 25 MPa. Dry green samples were raised to 1200 °C at the rate of 3 °C/min, sintered at that temperature for 4 h, then cooled to room temperature by turning off the working electric furnace. The samples of the monazite glass–ceramic wasteforms were characterized by homogeneous color, good shape, as well as no bubbles and cracks on their surfaces.

The monazite glass–ceramic samples were examined by a X-ray powder diffractometer (XRD, Cu Kα; PHILIPS X' Pert, Holland) to evaluate crystalline phase; and by an electron probe microscopic analysis (EPMA; JEOL JAX-8800R, Japan) technique to probe into phase species, phase abundances, phase composition, and grain shape, size and distribution of each phase; and by Fourier transform infrared (FTIR; Nicolet 550-Sereies II, USA) absorption spectra to detect phosphate glass species; and by differential scanning calorimetry (DSC; NETZSCH STA 409PG/PC, Germany) technique to scan glass transformation (T_g); and by Mössbauer spectra (radioactive source: 50mCi Co57/Pd; OXFORD-MS500, UK; fitting program: MOSFUN) to determine both the valances and the coordination numbers of iron ions; and by the imaging software, Image-Pro® Plus to analyze the volume fractions of the phases in the monazite glass–ceramics.

Table 2
Compositions of two simulated α-HLWs (wt%)

Element	1# HLW	2# HLW	Oxide	1# HLW	2# HLW
Fe	6.97	6.43	Fe_2O_3	7.83	7.42
La	29.36	27.09	La_2O_3	27.07	25.64
Ce	38.84	35.85	CeO_2	37.52	35.53
Mo	10.24	9.45	MoO_3	12.08	11.44
Zr (=TRU)	14.59	0.19	ZrO_2	15.49	0.21
Nd (=TRU)	0	20.99	Nd_2O_3	0	19.76
Total	100.000	100.00		100.00	100.00

Based on the Archimedes principle, a procedure defined by ASTM C373 [17] was adopted to calculate bulk density (D_B), apparent porosity (P_A), and water absorption (A_W) in the wasteforms, where D_B, P_A and A_W were calculated through the following equations:

$$D_B = D/(W - S), \tag{1}$$

$$P_A = (W - D)/(W - S), \tag{2}$$

and

$$A_W = (W - D)/D. \tag{3}$$

In these wasteforms D was for the dry weight of a sample, W for its wet weight in the air, and S for its wet weight in the water.

The chemical stability of the monazite glass–ceramics was evaluated from the dissolution rate (DR) in deionized water at 90 °C for 3 and 7 days. The rectangular samples, whose surface areas ranged between 450 and 550 mm^2, were cut from the simulated wasteforms, then polished and measured; and the finished samples were placed in the tightly closed Teflon containers, where a sample surface area-to-deionized water volume (S/V) ratio was 10 m^2/m^3. DR was calculated as

$$DR = \Delta W/dS, \tag{4}$$

where ΔW was for the difference between the weights of a sample before and after the dissolution test, d for the day, and S for the sample surface area.

3. Results and discussion

3.1. Characteristics of the phases in the monazite glass–ceramics

In Fig. 1, XRD powder patterns of the monazite glass–ceramic wasteforms, using 1 and 2 for W1 and W2, respectively, show that W2 contains one crystalline phase, namely monazite (JCPDS

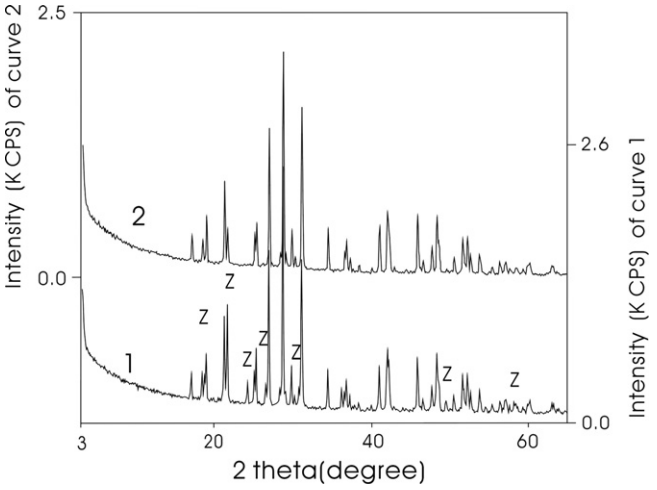

Fig. 1. XRD patterns of the monazite glass–ceramics. 1 for W1 and 2 for W2. Peak Z from ZrP_2O_7, and the peaks without any mark from monazite.

No 32-0199 and 32-0493), but W1 two crystalline phases, namely monazite and ZrP_2O_7 (JCPDS No 24-14903).

In Fig. 2, the electron backscattering images like A, B and C, collected from W1, show that W1 consists of five phases: the white granulous phase monazite designated M, the light gray granulous phase crystalline ZrP_2O_7 designated by Z, the gray amorphous phase molybdenum iron phosphate glass designated Gg, the black amorphous phase aluminum iron phosphate glass designated Gb, and the light gray amorphous phase zirconium phosphate glass designated Gg1. In Table 3, the compositions of the five phases of W1 are listed. The sharp boundary between phases Gg and Gb in Fig. 2(A) and (B) indicates that they are immiscible. In Fig. 2(B), the location of a Gg1 grain in phase Gg away from the boundary between phases Gb and Gg demonstrates that the glass phases Gg1 and Gg are immiscible. In Fig. 2(C), Z grains are cemented by glass Gg1.

The electron backscattering image in Fig. 2(D), collected from W2, shows that W2 consists only of three phases like M, Gg and Gb, whose compositions are listed in Table 3 .

There are small numbers of pores (the dark black area marked by P in Fig. 2(A) and (D)) in both W1 and W2.

Monazite grain sizes in W1 and W2 were in ranges of 2.29–9.14 μm and 2.86–5.71 μm, respectively, but compared with those in W1 monazite grain size in W2 was more uniform. Most of the monazite grains contained small round inclusions (see Fig. 2), which were too small to be analyzed by EPMA. Based on the electron backscattering images (400×) of two wasteforms, image analyses reveal that W1 was made up of 47.02% monazite, 42.77% glasses (including phase ZrP_2O_7), and 10.20 vol.% pores, and the corresponding volume percentages for phases in W2 are 66.54%, 26.14% and 7.32 vol.%, respectively.

When phosphate materials changed from ultraphosphate (mole ratio O/P < 3) to metaphosphate (O/P = 3), then to pyrophosphate (O/P = 3.5), finally to orthophosphate (O/P = 4), the quantity of active oxygen in their phosphate anion groups increased all through the process, which enhanced the oxidization in the phosphate series. Thus the O/P ratio of a phosphate material could predict how much the redox of the series worked. With the enhancement of

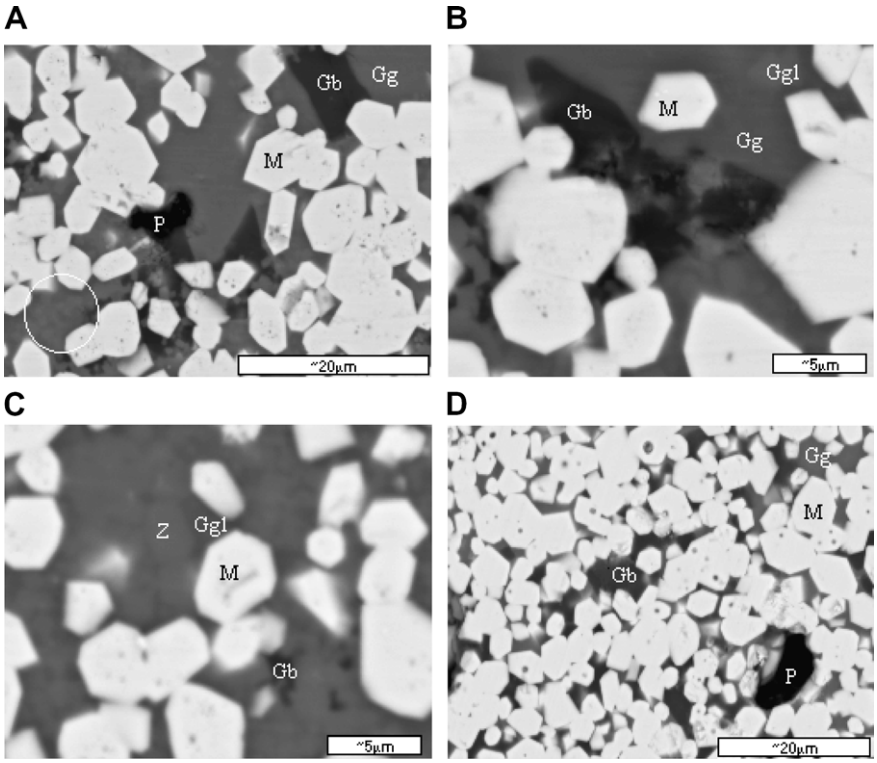

Fig. 2. The backscattering images for W1 and W2, namely images A, B and C for W1, and D for W2, M for monazite, Z for crystalline ZrP_2O_7, Gb for aluminum iron phosphate glass, Gg for molybdenum iron phosphate glass, Gg1 for zirconium phosphate glass, and P for pore. Image in the circle on the left hand bottom corner of image A shows that a granular phase with blurred outlines is included in phase Gg. Image B shows that a Gg1 grain with a blurred outline is included in Phase Gg. Image C shows the Z grains are cemented by the glass Gg1. W1 consists of the phases like M, Z, Gb, Gg, Gg1and P, and W2 consists of the phases like M, Gb, Gg and P.

Table 3
Compositions of monazites and glasses in two wasteforms[a] (EPMA, wt%)

Phase	Al_2O_3	P_2O_5	FeO	ZrO_2	MoO_3	La_2O_3	Ce_2O_3	Nd_2O_3	Total	O/P[b]
1-M	0.18 ± 0.03	30.18 ± 0.22	0.36 ± 0.09	0.04 ± 0.04	0.56 ± 0.1	46.48 ± 1.00	22.45 ± 0.89	0.15 ± 0.06	100.41 ± 2.43	4.0
1-Gb	17.92 ± 1.13	54.42 ± 0.75	20.16 ± 0.55	1.04 ± 0.61	2.68 ± 0.52	3.46 ± 0.71	1.38 ± 0.29	0.05 ± 0.03	101.11 ± 4.59	3.7
1-Gg	1.85 ± 0.06	46.69 ± 0.27	18.58 ± 0.10	0.00 ± 0.00	32.74 ± 0.14	1.23 ± 0.22	0.49 ± 0.12	0.04 ± 0.03	101.62 ± 0.94	4.0
1-Gg1	1.06 ± 0.42	50.42 ± 0.56	7.95 ± 0.28	24.33 ± 1.33	13.54 ± 1.05	1.79 ± 0.92	0.95 ± 0.22	0.04 ± 0.04	100.08 ± 4.82	3.7
1-Z	0.06 ± 0.031	54.31 ± 0.726	2.96 ± 0.501	34.90 ± 1.55	5.67 ± 0.52	1.39 ± 0.61	0.71 ± 0.16	0.01 ± 0.01	100.01 ± 0.02	3.5
2-M	0.11 ± 0.02	30.09 ± 0.12	0.18 ± 0.06	0.00 ± 0.00	0.45 ± 0.15	52.46 ± 0.26	8.00 ± 0.15	9.63 ± 0.10	100.92 ± 0.86	4.0
2-Gb	14.49 ± 0.71	51.66 ± 0.70	25.56 ± 1.28	0.00 ± 0.00	1.71 ± 0.21	6.5 ± 1.11	0.86 ± 0.16	1.17 ± 0.18	101.95 ± 4.35	3.7
2-Gg	1.48 ± 0.04	45.80 ± 0.23	21.02 ± 0.15	0.00 ± 0.00	29.71 ± 0.23	2.21 ± 0.29	0.29 ± 0.04	0.31 ± 0.08	100.82 ± 1.06	4.0

[a] Data in the table are the averages from several analyzing points: namely 1-M 9 points, 1-Gg 7 points, 1-Gg1 4 points, 1-Z 4 points, 1-Gb 12 points, 2-M 10 points, 2-Gg 8 points and 2-Gb 8 points.
[b] Mole ratio.

oxidization in the phosphate series, the transition ions therein would be in high valance when their quantity was definite. The O/P values in Table 3 show that phases M and Z belong to orthophosphate and pyrophosphate respectively, the glass phase Gg to orthophosphate, and the other two glass phases Gb and Gg1 to the category between pyrophosphate and orthophosphate. The high O/P values of the glass phases show that the monazite glass–ceramics are highly oxidized.

In Table 3, the majority of La^{3+}, $Ce^{3+}$and Nd^{3+} ions in the HLWs were immobilized in the monazite phase, and Zr^{4+} ions in both the crystalline ZrP_2O_7 and the zirconium pyrophosphate glass, which implies that TRU^{3+} ions might be immobilized in the monazite phase and TRU^{4+} in both crystalline pyrophosphate and pyrophosphate glasses.

Component Al, together with Fe and P formed stable Al–Fe–P–O quaternary glass Gb and likewise component Mo, together with Fe and P formed stable Mo–Fe–P–O quaternary glass Gg. When Al, Mo, Fe, P and O coexisted in a system, they would form two immiscible glass melts, e.g., phases Gg and Gb, instead of a homogeneous one. Component ZrO_2 was excluded from phase Gg in all cases, and the quantity of ZrO_2 allowed into phase Gb was not more than 1.6 wt%. As the amounts of MoO_3 and FeO were as high as 13.54 ± 1.05 wt% and 7.95 ± 0.28 wt%, respectively as shown in Table 3, they, together with 24 wt% of ZrO_2, formed the zirconium pyrophosphate glass (Gg1) which was immiscible to phase Gg, and when the content of ZrO_2 was more than 24.33 wt%, the crystallization of ZrP_2O_7 crystals occurred in zirconium pyrophosphate melt.

3.2. Infrared absorption spectra (IR) of the wasteforms

The main absorption bands of IR spectra of two monazite glass–ceramics (see Fig. 3) are consistent with those of natural monazite [18], namely three $F_2^{(2)}$ bands of $[PO_4]^{3-}$ at 1092–1090 cm^{-1}, 1059–1056 cm^{-1}, 1019–1017 cm^{-1}, respectively; A_1 band of O–P at 995–997 cm^{-1}, two bands of Ln–O at 946–947 cm^{-1} and 618–618 cm^{-1}, respectively; and two to three $F_2^{(1)}$ bands of $[PO_4]^{3-}$ at 561 cm^{-1} and 538–541 cm^{-1} [19,20], respectively. The band around 1270 cm^{-1}, characteristic band for the metaphosphate glass [21,22], is not visible in Fig. 3. Based on the fact that the bands between 720–780 cm^{-1} and 880 cm^{-1} were from symmetric stretching vibration and asymmetric stretching vibration of P–O–P in $[P_2O_7]^{4-}$ of pyrophosphate glass, respectively [23–25], and that neither of the crystalline ZrP_2O_7 [26] and the IR spectrum for W2 had the band at 746 cm^{-1}, we deduce that the band at 746 cm^{-1} in the IR spectrum for W1 comes from the phase Gg1, and that there is not any $[P_2O_7]^{4-}$ in W2.

Only when the $MoO_3/(MoO_3 + P_2O_5)$ ratio (mole) was equal to and more than 0.8 would the IR absorption bands from tetrahedral $[MoO_4]^{2-}$ appear [27]. Since the $MoO_3/(MoO_3 + P_2O_5)$ ratios of W1 and W2 are 0.41 and 0.39, respectively, and without any evidence for the existence of $[MoO_4]^{2-}$ in W1 and W2, we tend to understand that Mo^{6+} plays a role of network modifier in our case.

3.3. Mössbauer spectra of the wasteforms

The Mössbauer spectra of W1 and W2 at the room temperature are shown in Fig. 4. Given in Table 4 are the speciation of the iron ions and hyperfine parameters calculated from the Mössbauer spectra. In Table 4, the isomer shifts (IS) and the quadrupole splittings (QS) show that there are no Fe^{2+} in W1 and W2 at all, and that the values of IS1, QS1 and IS2, QS2 indicate the existence of high spin Fe^{3+} in both 4-fold coordination $(Fe^{3+})_4$ and 6-fold coordination $(Fe^{3+})_6$ on the one hand, and the Area 1/Area 2 $(=(Fe^{3+})_4/(Fe^{3+})_6)$ ratios of the two wasteforms, which are 0.65 and 0.66, respectively, mean that the quantity of $(Fe^{3+})_6$ is nearly two times more than $(Fe^{3+})_4$ on the other.

The O/P ratios of all phases in W1 and W2, recalculated on the basis of our Mössbauer study, are given as follows: 1-M 4.05, 1-Gb 3.89, 1-Gg 4.23, 1-Gg1 3.77, 1-Z 3.50, 2-M 4.06, 2-Gb 3.98 and 2-Gg 4.25. It is concluded from these ratios that the substitution of Fe^{3+} for Fe^{2+} in compositions has no effect on the O/P ratios of the crystal phases like M and Z, and little effect on the glass phase Gg1, but an obvious effect on the glass phases Gg and Gb. The O/P ratio of phase Gb is nearly equal to 4 as an orthophosphate, and an O/P value of 4.23–4.25 for the glass phase Gg shows that the quantity of P^{5+} ions would not be enough to form an orthophosphate network

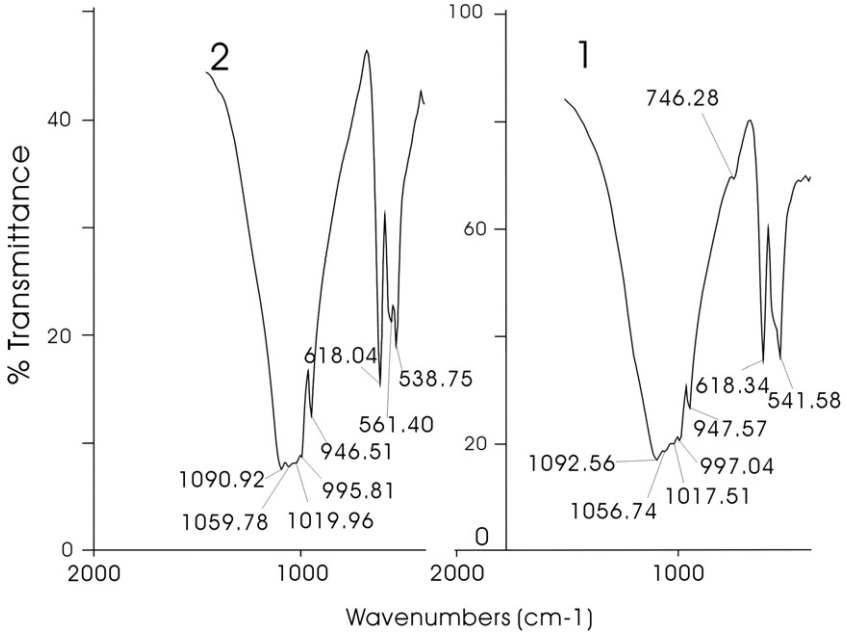

Fig. 3. FTIR spectra of two wasteforms. 1 for W1 and 2 for W 2.

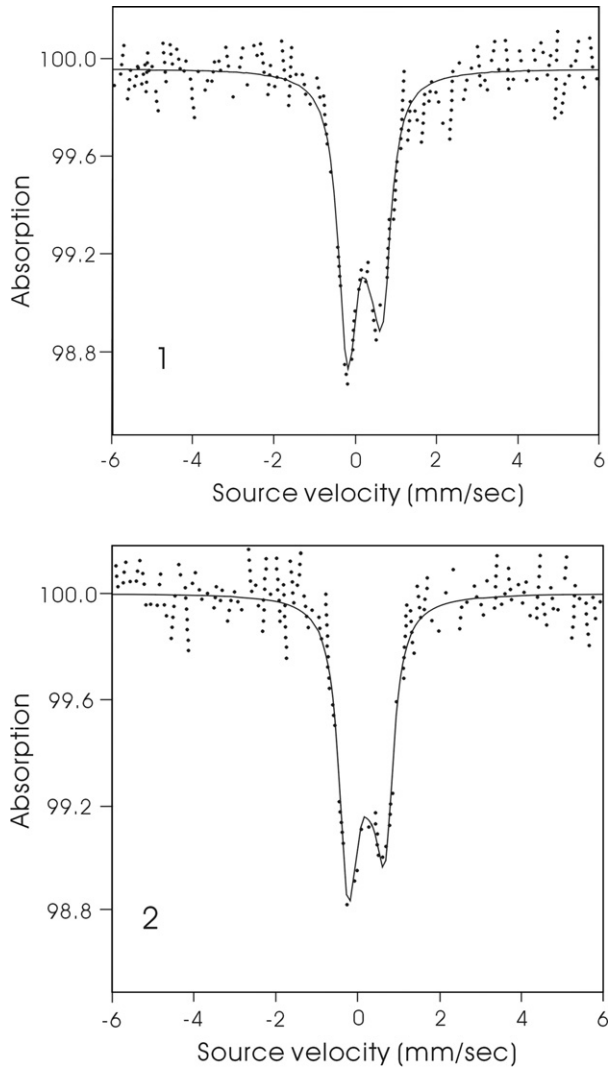

Fig. 4. Mössbauer spectra of two monazite glass–ceramics at the room temperature. 1 for W1 and 2 for W2.

Table 4
Mössbauer hyperfine parameters of W1 and W2 at the room temperature

Wasteform	IS1	QS1	IS2	QS2	$(Fe^{3+})_4$[a]	$(Fe^{3+})_6$[b]	$(Fe^{3+})_4/(Fe^{3+})_6$
W1	0.2803	0.4006	0.3445	0.9297	724.98	1120.54	0.65
W2	0.2847	0.4639	0.3616	0.8927	768.46	1166.84	0.66

[a] Fe^{3+} in 4-fold coordination.
[b] Fe^{3+} in 6-fold coordination.

even if all bridging oxygen were broken up in the phosphate network.

Considering the Fe^{3+} ions in 4-fold coordination as tetrahedron $[FeO_4]^{5-}$ for $[PO_4]^{3-}$ in a glass network, the $O/(P + 1/3Fe^{3+})$ ratios of the glasses are as such, 1-Gb 3.47, 1-Gg 3.74, 1-Gg1 3.58, 2-Gb 3.42 and 2-Gg 3.69, which fluctuate around an O/P value of 3.5. Although the $O/(P + 1/3Fe^{3+})$ ratios were not reasonable from the unknown definite quantities of the $(Fe^{3+})_4$ in each glass phase, it was shown at the least that the substitution of $[FeO_4]^{5-}$ for $[PO_4]^{3-}$ would possibly occur in the networks of these kinds of phosphate glasses, whose O/P ratio was more than 4, and that these glasses were in a highly oxidized state.

3.4. Glass transition temperatures (T_g) of the wasteforms

In Fig. 5, the stronger endothermic reaction in the DSC curve of W1 results from its higher content of glasses. Two endothermic peaks are at 588 °C and 880 °C on the DSC curve for W1, but only one endothermic peak at 612 °C on the curve for W2. Therefore we believe that two T_gs, which are at the peak of 588 °C on curve 1 and at the peak of 612 °C on curve 2, come from the mixtures of the glasses Gg and Gb in W1 and W2, respectively, and that one T_g at the peak of 880 °C on curve 1 comes from the glass Gg1 in W1 since the phases Gg and Gb exist in both W1 and W2 and the phase Gg1 does only in W1.

Generally, the higher the T_g of a glass phase is, the higher its crystallizing temperature and its thermal stability will be. Compared with the T_gs in the ranges of 400–500 °C of iron phosphate glasses [5,8,21], the T_gs of the glass phases in W1 and W2 are much higher, which mean that the wasteforms will have higher thermal stability.

3.5. Dissolution rates of the wasteforms

In Table 5, the bulk densities, apparent porosities and water absorptions of W1 and W2 are listed. The P_A and A_W values show that W1 is denser than W2 because of its higher glass content. Larger bulk density of W2 results from its higher content of Nd rather than Zr.

The samples, cut from the same monazite glass–ceramic disc for the dissolution rate test, were ground through SiC powder and then polished by using diamond paste. After the polished samples were made clean by supersonic and dried, they were measured in terms of surface area by using a vernier caliper with a precision of 0.02 mm and from the five different measurements of their surface areas an average was taken. After their weights were gained before soaking, the finished samples, suspended within deionized water in the tightly sealed Teflon containers, were kept at 90 °C for 3 days and 7 days and then were taken out to be washed clean by deionized water and dried up and thus their weights after soaking were gained. Finally the dissolution rates (DR) of the samples were calculated through the Eq. (4). In Table 6, the relevant parameters for

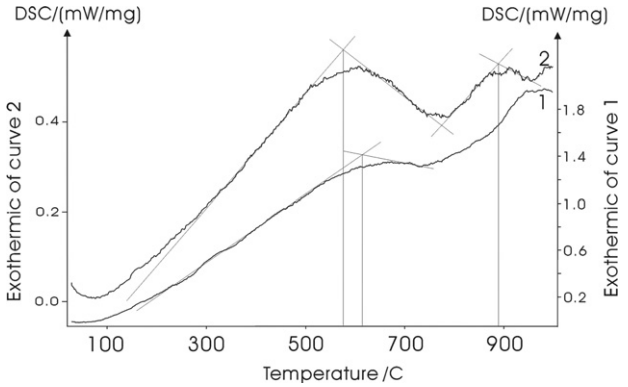

Fig. 5. DSC curves of two wasteforms. 1 for W1 and 2 for W2.

Table 5
Densities, porosities and water absorptions of the wasteforms[a]

Wasteform	D (g)	W (g)	S (g)	D_B (g/cm^3)	P_A (%)	A_W (%)
W1	2.3045	2.3061	1.7001	3.8028	0.26	0.07
W2	1.6962	1.7036	1.2740	3.9483	1.72	0.43

[a] Weight measuring error $\sigma \leqslant 0.5\%$.

Table 6
Sizes, weights and dissolution rates for the samples of two simulated wasteforms[a]

Simulated wasteform	Time (day)	Length (mm)	Width (mm)	Height (mm)	Area (mm^2)	Weight 1[b] (g)	Weight 2[c](g)	Weight loss (g)	DR (g/m^2d)
W1	3	16.72	11.27	3.87	593.51	2.6839	2.6831	0.0008	0.4493
	7	13.14	10.19	4.44	474.96	2.2113	2.2103	0.0010	0.3008
W2	3	16.03	10.90	3.27	571.36	2.2039	2.2034	0.0005	0.2917
	7	14.20	10.10	3.45	494.80	1.8993	1.8984	0.0009	0.2598

[a] Size measuring error $\sigma \leqslant 0.5\%$, and weight measuring error $\sigma \leqslant 0.5\%$.
[b] Weight before the test.
[c] Weight after the test.

the DR calculation of two wasteforms are listed. The DRs of 7-day tests of W1 and W2 are lower than those of 3-day ones, and both 3-day and 7-day DRs of W2 are all lower than those of W1, which shows that W2 has rather higher chemical durability than W1.

4. Conclusion

Two monazite glass–ceramic wasteforms were fabricated by mixing lanthanum metaphosphate glass powder with the oxide powder of the components in simulated α-HLW in which components transuranium elements were replaced by Nd and Zr, respectively. It was shown in our study that TRU^{3+} would be immobilized mainly by the monazite phase, and TRU^{4+} might evolve into both pyrophosphate crystals and pyrophosphate glasses of the transuranium elements. The glass phase T_gs in the wasteforms, prepared through this approach, were more than 588 °C, which suggests these glass phases possessed fairly strong resistance to crystallization.

When the iron phosphate melt contained components Al and Mo together, it separated into two immiscible glass melts, namely aluminum iron phosphate and molybdenum iron phosphate, which means that it is not possible for components Al and Mo to co-exist in an iron phosphate glass.

Iron in the glass phases of the wasteforms is in a state of high spin Fe^{3+}, one third of which is with a coordination number of four and the remaining two thirds with a coordination number of six. The O/P ratios, calculated on the basis of Fe^{3+}, of the glass phases are the following: the O/P ratio of zirconium phosphate glass(1-Gg1) is 3.77; that of aluminum iron phosphate glass (1-Gb and 2-Gb) 3.89 and 3.98, respectively; and that of molybdenum iron phosphate (1-Gg and 2-Gg) respective 4.23 and 4.25, which shows that the quantity of P^{5+} ions is not high enough to form an orthophosphate network and that the substitution of $[Fe^{3+}O_4]^{5-}$ for $[PO_4]^{3-}$ occurred in the glass network. The $O/(P + 1/3Fe^{3+})$ ratios of the same phases are as follows: 1-Gb 3.47, 1-Gg 3.74, 1-Gg1 3.58, 2-Gb 3.42 and 2-Gg 3.69. It is shown in the change from the O/P to $O/(P + 1/3Fe^{3+})$ ratios that the change of their valance will have an obvious effect on both the species and the redox condition of a phosphate glass when the amount of iron ions becomes large.

The quite low dissolution rates of the wasteforms fabricated by this approach in the present paper demonstrate that the glass phases in the monazite glass–ceramics are of high chemical stability.

References

[1] L.A. Boatner, B.C. Sales, in: W. Lutze, R.C. Ewing (Eds.), Radioactive Waste Form for the Future, Elsevier Science, North Holland, 1988, p. 495.
[2] B. Glorieux, M. Matecki, F. Fayon, et al., J. Nucl. Mater. 326 (2004) 156.
[3] W.P. Nash, in: J.O. Nriagu, P.B. Moore (Eds.), Phosphate Minerals, Springer-Verlag, Berlin, 1984, p. 215.
[4] G.K. Marasinghe, M. Karabulut, C.S. Ray, et al., J. Non-Cryst. Solids 263&264 (2000) 146.
[5] C.W. Kim, C.S. Ray, D. Zhu, et al., J. Nucl. Mater. 322 (2003) 152.
[6] W. Huang, D.E. Day, C.S. Ray, et al., J. Nucl. Mater. 327 (2004) 46.
[7] D.M. Zhu, CW. Kim, D.E. Day, et al., J. Nucl. Mater. 336 (2005) 47.
[8] X.Y. Fang, C. S Ray, G.K. Marasinghe, et al., J. Non-Cryst. Solids 263&264 (2000) 293.
[9] P. Hartmann, J. Vogel, U. Friedrich, et al., J. Non-Cryst. Solids 263&264 (2000) 94.
[10] R.C. Ewing, W.J. Weber, F.W. Clinard Jr., Prog. Nucl. Energy 29 (2) (1995) 3.
[11] D.W. Wheeler, P.D. Bdger, J. Alloy. Compd. 444&445 (2007) 212.
[12] N.J. Hess, W.J. Weber, S.D. Conradson, J. Alloy. Compd. 271–273 (1998) 240.
[13] P. Loiseau, D. Caurant, N. Baffier, et al., J. Nucl. Mater. 335 (2004) 14.
[14] C. Lopez, X. Deschanels, J.M. Bart, et al., J. Nucl. Mater. 312 (2003) 76.
[15] W.A. Deer, R.A. Howie, J. Zussman, Orthosilicates, Rosk-forming Minerals 2ED, vol. 1A, Longman Group Limited, London, 1982.
[16] I.W. Donald, B.L. Metcalfe, R.N.J. Taylor, J. Mater. Sci. 32 (1997) 851.
[17] ASTM Specification C373, ASTM Standards, Part 13, American Society for Testing and Materials, Philadelphia, 1969.
[18] Sadtler Research Laboratories, Minerals Infrared Grating Spectra, vol. 1, Sadtler Research Laboratories Inc., Philadelphia, PA, USA, 1973, p. MN175K.
[19] M. Rokita, M. Handke, W. Mozgawa, J. Mol. Struct. 555 (2000) 351.
[20] A. Adamczyk, M. Handke, J. Mol. Struct. 555 (2000) 159.
[21] H. Hirai, T. Masui, N. Imanaka, et al., J. Alloy. Compd. 374 (2004) 84.
[22] A. Chahine, M. Et-tabirou, J.L. Pascal, Mater. Lett. 58 (2004) 2776.
[23] A.M. Efimov, J. Non-Cryst. Solids 209 (1997) 209.
[24] N. Clavier, N. Dacheux, P. Martinez, et al., J. Nucl. Mater. 335 (2004) 397.
[25] C.G.S. Pillai, V. Sudarsan, M. Roy, et al., J. Nucl. Mater. 321 (2003) 313.
[26] K. Byrappa, I.I. Plyusnina, G.I. Dorokhova, J. Mater. Sci. 17 (1982) 1847.
[27] P. Znasik, M. Jamnicky, J. Non-Cryst. Solids 146 (1992) 74.